

Discrete Elastic Model for Two-dimensional Melting

Yves Lansac, Matthew A. Glaser and Noel A. Clark
*Condensed Matter Laboratory, Department of Physics, and
Ferroelectric Liquid Crystal Materials Research Center,
University of Colorado, Boulder, CO 80309, USA*
(Dated:)

Our previous molecular dynamic simulation studies of simple two-dimensional (2D) systems [1] suggested that both geometrical defects (localized, large-amplitude deviations from hexagonal ordering) and topological defects (dislocations and disclinations) play a role in 2D melting. To capture the main features of the 2D melting transition and investigate the respective roles of these two classes of defects, we study a discrete elastic model consisting of an array of nodes connected by springs, for which the relative number of geometrical defects (modeled as broken springs) and topological defects (nodes having a coordination number different from 6) may be precisely controlled. We perform Monte Carlo simulations of this model in the isobaric-isothermal ensemble, and present the phase diagram as well as various thermodynamic, statistical and structural quantities as a function of the relative populations of geometrical and topological defects. The model exhibits a rich phase behavior including hexagonal and square crystals, expanded crystal, dodecagonal quasicrystal, and liquid structure. We found that the solid-liquid transition temperature is lowered by a factor 3 to 4, with respect to the case when only topological defects are allowed, when both topological and geometrical defects are permitted, supporting our hypothesis concerning the central role played by the geometrical defects in the melting. The microscopic structure of the dense liquid has been investigated and the results are compared to those from simulations of 2D particle systems.

INTRODUCTION

The process of melting is one of the most common yet fascinating phenomena encountered in every day life. The abrupt changes in the properties of a substance when it is heating above its melting point, i.e. the dramatic change from solidity through fluidity, achieved with very small change in density, remain mysterious and intriguing. If modern statistical mechanics theory, through the integral equation [6] approach, allow to compute, although with approximation, the pair correlation function and the thermodynamics properties of dense liquid, it does not provide an intuitive microscopic picture of a dense fluid nor give an understanding of the entropy of a dense fluid or the entropy difference between the solid and liquid states.

In the 60's, a crystallographer, J.D. Bernal, tried to relate the structure of a liquid, not too far away from its freezing point, to excluded volume problem [2, 3, 4, 5]. In Bernal's view, a liquid is essentially homogeneous, coherent and irregular in opposite with a crystal which may be seen as a pile of molecules regularly arranged. His work consisted to determine the local organization of molecules in various mechanistic model governed by geometrical packing constraints and to identify the kind of polygons defined by the bonds binding the center of mass of neighbors particles, forming holes responsible of the less packing organization in a dense liquid in contrast to the close packing of solids. His approach was primarily descriptive, and was almost completely abandoned in favor of the modern integral equation approach. However, the present description shear a lot of idea with these earlier works because we think that this approach is an important way to develop a general description of melting theory and to provide a very intuitive picture of the structure and properties of a dense liquid.

In addition to the general understanding of the liquid structure, the two-dimensional (2D) case is even more puzzling due to the fact that no true long-range positional order is present [7, 8, 9]. Different theories predict that this difference in the nature of the 2D and 3D solid lead to a completely different melting mechanism. In particular, the theory developed by Kosterlitz and Thouless [10, 11] and extended by Halperin, Nelson [12, 13] and Young [14] (KTHNY) has received a lot of attention. According to their prediction, the solid-liquid transition in two dimensions occurs by the intermediate of two second order phase transitions, corresponding to the unbinding of dislocations and disclinations. In addition, a new phase called the hexatic phase is predicted to appear between the solid and the liquid. This phase is characterized by short-range positional order and by quasi long-range bond orientational order. A lot of work, both numerical and experimental have been done in order to probe this theory. However no strong evidence for the KTHNY theory has emerged from the theoretical studies, and the results from most of the simulations indicate that another melting mechanism preempts the KTHNY mechanism.

Our previous molecular dynamics (MD) simulations [1] performed in the microcanonical ensemble and based on a system of disks interacting via a soft repulsive potential have focused on the mechanism of melting and were devoted to a better intuitive understanding of the microscopic structure of a dense liquid. The results have shown that the

melting occurs via a first-order phase transition and that an important aspect of the transition is the appearance of geometrical (non topological) disorder in the liquid phase. This disorder manifests itself in the presence of a significant degree of square lattice coordination (holes, see Figure 1) in the liquid phase with particles adopting local arrangements characteristic of plane tilings composed of squares and equilateral triangles (ST tilings)[15, 16, 17]. Dense random packings (DRPs) [18, 19] exhibit the same kind of ST tiling like structures and are quite supportive of the fact that geometrical constraints play an important role in melting and the liquid structure. Topological defects are responsible for the loss of long-range positional order characteristic of a liquid, but the geometrical excitations, not captured by the Voronoi [20] or Delaunay (the dual of the Voronoi representation) representations, formed by almost local square organization of the particles may contribute significantly to the thermodynamics (i.e the change in density) occurring at the melting transition. Both topological and geometrical defects are the fundamental excitations which control the transition and formed the basis the basis of our mechanistic picture of a dense liquid: the two-dimensional melting is a condensation of localised, thermally generated geometrical and topological defects. Condensation is a phase transition resulting from attractive interactions between the excitation or particles of interest, i.e. in our case between the defects. The scalar order parameter of the transition (i.e. the number density of geometrical defects) is unrelated to the symmetry-derived order parameters and then the global symmetry change could be very well seen as a side effect of the defect condensation mechanism which drives the 2D melting transition. This picture is similar to the one obtained in a three-dimensional liquid by the mechanistic models of Bernal. This is not too surprising, because in the framework of a melting transition driven mainly by packing constraints, global symmetry is irrelevant in determining the characteristics of the melting transition, then there is no compelling reason that 3D melting should be qualitatively different from 2D melting.

Based on these observations, we present here a discrete elastic model constituted by a network of nodes connected together by elastic springs which capture the essential features of the structure of a liquid not too far from the freezing point. This model can be seen as an analog of the mechanistic models from Bernal, modern computer and Monte-Carlo techniques allowing to have a much more powerful tool to probe the statistical structure of liquids.

In the first part of the article, we describe the discrete elastic model and the numerical methodology applied in order to mimic a dense liquid.

In the second part we present the phase diagrams obtained with the model as a function of the relative populations of the two different kind of excitations. Then the structure of the dense liquid is discussed in detail and various thermodynamical and structural quantities are computed and compared with our earlier simulations, hereafter referred as WCA liquid.

In conclusion we discuss the pertinence and limitations of our model as well as the possible extensions and applications, in particular to freely suspended liquid crystal thin films.

DISCRETE ELASTIC MODEL

From the WCA liquid study, the 2D melting can be seen as a defect condensation transition involving both geometrical and topological defects.

Topological defects (disclinations) are characterized by a number of nearest-neighbors different from 6 (i.e, different from what is expected for a perfect triangular lattice). A node (playing in our model the role of the center of mass of a disklike particle) having 5 nearest-neighbors is identified as a -1 disclination due to the fact that it corresponds to the removal of a 60° wedge of material at a microscopic level, while a node having 7 nearest-neighbors is identified as a +1 disclination, corresponding to the addition of a 60° wedge of material at a microscopic level. An isolated disclination corresponds to the 60° rotation of a vector oriented along one of the lattice direction upon parallel transport around a closed circuit enclosing the disclination and is responsible for the loss of long-range bond-orientational order in the system. An isolated dislocation is formed by a bound pair of disclination of opposite strength and corresponds to a non-zero Burger vector (the amount by which a Burger's circuit fails to close around a dislocation) and is responsible for the loose of quasi-long-range positional order in the system. In the liquid phase, a Burger's circuit is a ill-defined quantity since no lattice is present.

Geometrical defects are non-topological defects and large amplitude localized geometrical distortions in which the particles have adopted a nearly square organization but are not associated with a disclination or dislocation (see Figure 1). There is a clear tendency for particles in the dense 2D WCA liquid to form local arrangements characteristic of ST tilings. The WCA liquid can be usefully describe as polygon packings or imperfect tilings (i.e. formed with deformable tiles), and the effect of packing constraints on the local geometry of these dense systems can be embodied in particular tiling rules that condition the local arrangement of the polygons. The volume increase upon melting is directly related to the creation of polygons having more than 3 sides.

The discrete elastic model is built to mimic the polygon tiling representation obtained from the Delaunay representation in the WCA liquid and to reproduce the two kinds of excitations responsible for the melting transition and the dense liquid structure. It is constituted by a network of nodes (playing the role of the center of mass of the disk particles of the WCA liquid) connected by springs. In addition to the bond stretching springs, bond angle bending springs have been considered in order to avoid unphysical folding of the network at high pressure (Figure 2). A solid-like local structure is characterized by a triangular equilateral network of springs connecting nodes, or equivalently by a plane tiling of nearly perfect equilateral triangles. One of the main interests of the model over its real-particle counterpart is that it is possible to probe almost independently the effect of topological and geometrical excitations on the melting transition and the resulting dense liquid structure.

Within the framework of the discrete elastic model, the creation of topological defects is reproduced by a local change in the connectivity of the network achieved by the flipping of a given spring bond between two nodes. The network topology is locally modified, resulting in the creation of a bound-pair of dislocations (Figure 3a). Such a neutral quadrupole arrangement does not disrupt the long-range positional order of the system, but is at the origin of the subsequent creation of topological defects by unbinding mechanism. The creation of isolated dislocations then isolated disclinations from such a quadrupole is schematically depicted on Figure 3a.

The creation of a geometrical defect is achieved by a bond breaking (Figure 3b). This procedure allows the two previously connected nodes to remain in the proximity of their former nearest-neighbors without being strongly bound to them, behaving as nearly as second-neighbors. This is a weaker effect than the change of neighborhood induced by a bond flipping. Practically, the bond breaking procedure is accompanied by an update of the equilibrium bond angles to reflect the induced change in geometry from two equilateral tiles (bond angle springs set to 60°) to one nearly-square tile (bond angle springs set to 90°) (Figure 3b).

These two procedures (bond flipping and bond breaking) are suitable to mimic a system in which the populations of the two kinds of defects can be controlled and their resulting effects on the melting transition analysed. If only bond flipping is allowed, we will talk about an only topological model, if only bond breaking is allowed, the model will be qualified of only geometrical model and if both bond flipping and bond breaking are permitted, we will talk of a topological and geometrical model. It is worth noticing, however, that local, square-like fluctuation of the triangular lattice are also present in the only topological model, and could be exhibited by using a bond dilution procedure (*i.e.* removal of all the bonds significantly longer than the average bond length present in the network). However, these fluctuations are, due to the constraints imposed on the model, much less favorable energetically than in the model where bond breaking is allowed. This is in this sense that a distinction has been made between the only topological model and the topological and geometrical model.

Our model can handle the creation of geometrical defects up to six sides polygons (hexagonal tiles) and the creation of topological defects of different strength (*i.e.* with different coordination numbers) but in this article we focus on the minimal model in which only triangular and square tiles (3 and 4-sides polygons) and topological defects with 5 and 7 coordination numbers are considered. This is in agreement with the extensive studies performed on the WCA liquid and the random close packing system in which it was demonstrated that these excitations are the most relevant ones.

The Hamiltonian for this system is:

$$H = \frac{K_r}{2} \sum_{i,j} (\mathbf{r}_{i,j} - \mathbf{a})^2 + \frac{K_\theta}{2} \sum_{i,j,k} (\theta_{i,j,k} - \theta_p)^2 + PA \quad (1)$$

where the first sum is on all non-broken bonds and the second on all the bond-angle between non broken bonds, $|\mathbf{a}| \equiv a$ is the equilibrium length between the two connected nodes i and j and θ_p is the equilibrium bond angle between nodes i , j and k , for the polygon p considered ($\theta_p = 60^\circ$, for $p = 3$ *i.e.* for an equilateral triangle polygon and $\theta_p = 90^\circ$, for $p = 4$ *i.e.* for a square polygon). In the case when both topological and geometrical defects are allowed no energetic cost is associated with the flipping of a broken bond. That is related to the fact pointed above, that a quadrupole of defects is nearly topologically equivalent to no defects. K_r is the stretch elastic constant, K_θ the bend elastic constant, A the area of the system and P the external pressure.

The properties of the elastic model depend only on three dimensionless parameters, a reduced temperature t , a reduced elastic constant ratio K and a reduced pressure p defined as:

$$t = \frac{k_B T}{K_r a^2} \quad (2)$$

$$K = \frac{K_\theta}{K_r a^2} \quad (3)$$

$$p = \frac{P}{K_r a^2} \quad (4)$$

where k_B is the Boltzman constant and T the temperature of the system.

The statistical mechanical properties of the discrete elastic model are investigated using Metropolis Monte Carlo (MC)[23] simulations carried out in the isobaric-isothermic ensemble. Translational node displacements are also considered in order to relax the local strain induced in the system by the creation of defects resulting in a network connectivity change. In addition, the simulation box area is allow to fluctuate in order to insure a constant pressure in the system.

PHASE DIAGRAMS

In order to check the ability of our model to reproduce the solid-liquid transition and in order to probe the relative importance of the two kind of excitations in our model, we compute the (p, t) phase diagrams corresponding to the cases when only geometrical, only topological, both geometrical and topological defects are allowed. A system with $N = 100$ nodes and then $3N$ bonds is used. Additional simulations have been carried out for selected state points with a larger system with $N = 1024$ nodes in order to assess finite size effects and their influence on the location of the phase boundaries. A value $K = 0.1$ has been chosen for all the considered models. The effect of an increase of the elastic network stiffness will result in an increase in the liquid-solid transition temperature and its effects on the location of other phase boundaries will be study in another work.

At each state point (p, t) , a Monte-Carlo sampling is used corresponding to 200000 sweeps for equilibration and 10^6 sweeps for production. The rough location of the phase boundaries is obtained upon heating the system by successive steps Δt . Smaller steps in temperature are subsequently used in order to refine the phase boundary location. Every sweep consist in the attempting move of the N nodes, attempting move of the $3N$ bonds (i.e. only flipping in the case when only topological defects are considered, only breaking when only geometrical defects are considered and either breaking or flipping when both kind of excitations are presents) and one attempting move of the simulation box (either only the area, or only the shape or a combination of the two precedent kind) in order to keep a pressure fluctuating around the specified value.

For each pressure, the location of the phase transition as a function of the reduced temperature, and the structure of the phases are determined by computing the equation of state, the energy, the specific heat and the magnitude of the bond-orientational order parameters. Various bond-orientational order can be characterized by considering, in a general way, a bond angle density for a particle (node) i defined as;

$$\rho_{bi}(\theta) = \frac{2\pi}{n_i} \sum_{j=1}^{n_i} \delta(\theta - \theta_{ij}) \quad (5)$$

where the sum runs over the n_i nearest-neighbors of particle i and θ_{ij} is the angle of the bond between particle i and its j th neighbor with respect to a reference direction. Because $\rho_{bi}(\theta)$ has a periodicity of 2π , we can write a Fourier decomposition:

$$\rho_{bi}(\theta) = \sum_{m=0}^{\infty} \psi_{mi} \exp(-im\theta) \quad (6)$$

where the complex Fourier coefficients ψ_m are given by:

$$\psi_m \equiv \psi_{mi} = \frac{1}{n_i} \sum_{j=1}^{n_i} \exp(im\theta_{ij}) \quad (7)$$

plays the role of a m -fold local bond orientational order parameter. In addition we can define a global m -fold order parameter:

$$\Psi_m = \frac{1}{N} \sum_{i=1}^N \psi_m \quad (8)$$

which gives a signature of the global m -fold order present in the system. We focus here on Ψ_4 , Ψ_6 and Ψ_{12} which are respectively sensitive to squarelike solid phase, triangular solid phase and dodecagonal quasicrystalline phase. A liquid phase will be characterized by negligible magnitudes of these three order parameters.

The resulting phase diagrams corresponding to the only geometrical model, the only topological model and the topological and geometrical model are presented respectively on Figure 4a, b and c.

When only geometrical defects are allowed (Figure 4a) no change in symmetry is expected. The system exhibits an hexagonal crystal phase (X_h), an expanded hexagonal crystal (EX) i.e. an hexagonal crystal with a lower density to the presence of a significant number of geometrical defects (square-like fluctuations) and a quasicrystalline (QX) phase (dodecagonal, formed by perfect ST tiling [24, 25, 26, 27]). A triple point (X_h , QX, EX) is located around $p \simeq 0.03$ and $t \simeq 0.0068$. The crystal-expanded crystal transition is similar to a liquid-gas phase transition and therefore is first order and end by a critical point located around $p = 0.055$. The location of this phase boundary has been characterized by the apparition of a sharp peak in the variation of the specific heat with the temperature. A representative configuration of the expanded crystal is shown on Figure 6.

The location of the critical point has been achieved by performing additional simulations with the $N = 1024$ system at a pressure $p = 0.05$ and $p = 0.07$. At this latter pressure no discontinuity in the order parameters or peak in the specific heat is noticeable. At pressures lower than $p = 0.03$ a quasicrystalline phase is stabilized. The relative stability of the hexagonal crystal phase (i.e a perfect tiling of the plane with equilateral triangular tiles) and the dodecagonal quasicrystalline phase (i.e. a perfect tiling of the plane with equilateral triangular and square tiles) arises as a competition between the entropy of configuration (the different arrangement of the tiles) - and to a lesser extend the entropy of vibration of the nodes - and the enthalpy (the volume change). At low enough pressure, the gain in entropy induced by a quasicrystalline phase overcomes the increase in volume for a given range of temperature ($0.005 < t < 0.0071$, at $p = 0$), stabilizing the QX phase. As expected the range of stability of the QX phase with respect to the crystal phase decreases when the pressure increases. As shown for $p = 0.02$, finite-size effects seem to increase the range of stability (vs. the crystal phase). A representative configuration ($p = 0.02$ and $t = 0.0064$) of the dodecagonal quasicrystalline phase is shown on Figure 7. The number of square polygons divided by the number of triangle polygons is ~ 0.44 and is constant within the full temperature range ($0.006 < t < 0.007$) of existence of the quasicrystal phase at $p = 0.02$. This value is in good agreement with the value ($\sqrt{3}/4$) obtained with random tiling models (which cover the plane with a set of rigid tiles without gap) when the fraction of total tiling area occupied by square tiles is equal to the fraction occupied by triangle tiles, i.e when the system exhibit twelvefold rotational symmetry. At the same reduced pressure, the ratio square tiles over triangle tiles is ~ 0.41 for the $N = 100$ nodes system. Finite-size effects seems to decrease the probability of occurrence of geometrical defects.

The model when both topological and geometrical defects are allowed (Figure 4c) exhibits a richer phase behavior than the only geometrical model with the presence of a hexagonal crystal (X_h) phase, a square crystal (X_s) phase, a dodecagonal quasicrystal (QX) phase and a liquid (L) phase. Typical examples of these phases are shown on Figure 7. Two triple points are present, a (QX , X_s , L) located around $p \simeq 0.03$ and $t \simeq 0.0065$ and a (X_h , QX, L) triple point located around $p \simeq 0.06$ and $t \simeq 0.006$. If we make abstraction of the presence of the square crystal phase and we extend the upper phase boundary of the quasicrystalline phase toward $p = 0$, we notice that the temperature range of existence of the quasicrystalline phase is comparable to the one present in the only geometrical model. However, the stability range in pressure of the quasicrystalline phase is almost twice as large as in the only geometrical model, due to the presence of topological defects which allow a larger gain both in entropy of conformation (by introducing tiling faults) and in entropy of vibration. By comparison with the only geometrical model, the number of square tiles divided by the number of triangle tiles is around ~ 0.45 in the quasicrystalline phase, at $p = 0.02$ for the system with $N = 100$ nodes. At $p = 0.01$ and $p = 0.04$, for the $N = 1024$ system, the ratio square/triangle is roughly in the range $\sim 0.43 - 0.44$. Quite surprisingly, for pressure lower than $p \simeq 0.03$, a square crystal phase preempts, at high enough temperature, the full apparition of the quasicrystalline phase. This phase seems to become energetically favorable with respect to both the quasicrystalline phase and the liquid phase and quite interestingly is not present for the only geometrical model. It seems likely that this is due to a feature of the elastic model, in which a bond entropy is contributing to the total entropy of the system. Because a broken bond is free to flip without any energy cost, the gain in bond entropy overcomes the loss in entropy of configuration and the increase in volume and stabilize the square

crystal with respect to the quasicrystal and the liquid phase at low enough pressure and high enough temperature. This is probably the same reason which leads, at the same pressure ($p = 0.02$) and for the same temperature range, the quasicrystalline phase of the only geometrical model to exhibit slightly less squarelike polygons than the topological and geometrical model. For pressures larger than $p \simeq 0.06$ a transition between an hexagonal crystal and a dense liquid occurs. The change in symmetry of the system is governed by the topological defects. Studies at $p = 0.08$ with the $N = 1024$ nodes system seem to indicate that the location of the solid-liquid phase boundary is not very sensitive to finite-size effects.

The only topological phase diagram (Figure 4b) exhibits a hexagonal crystal phase (X_h) and a dense liquid due to the presence of topological defects. A phase transition between these two phases occurs over the full range of pressures studied. At each pressure, a well defined peak in the specific heat appears at the transition but due to finite size effects it is difficult to probe the nature of the transition. The phase diagram reported here has been computed upon heating. No significant hysteresis has been observed upon cooling. Studies carried out for the larger system $N = 1024$ at $p = 0.02$ and $p = 0.08$ indicate that the location of the phase boundary is shifted upward due to finite-size effects. Typical examples of the liquid phase are presented on Figure 7, for a temperature close to the melting point and for a temperature deeper into the liquid phase. It is interesting to notice, from the ‘slope’ of the solid-liquid phase transition line, using the Clapeyron relation, that our model lead to the formation of a liquid denser than its solid phase. Even if this feature is not uncommon for real liquids, it seems that in our case, this effect is related to the intrinsic nature of the discrete model. Topological defects seem to create local compressible regions, increasing the density in the system. On the phase diagram is also reported the predicted theoretical phase transition (see Appendix) from the Kosterlitz-Thouless (KT) model which corresponds to the unbinding of pairs of dislocations. It is thought to be the upper limit for the transition to occur if no other mechanism preempts it. We notice that the KT prediction for our model is around two times larger than the transition temperatures obtained from the elastic model simulation. However, our estimation have been done at $T = 0$ and taking into account the topological defects will decrease sensitively the predicted values.

The most striking feature of the phase diagrams presented in Figure 4 is the dramatic decrease (by a factor three to four) in the solid-liquid transition temperature upon inclusion of geometrical (as well as topological) defects. Evidently, the geometrical defects significantly stabilize the liquid phase relative to the solid phase. This is the potential energy per node $u = U/N$ which mainly set the scale of the solid-liquid transition temperature. At $p = 0.08$ and $N = 1024$ the difference in potential energy per node at the transition $\Delta u(t_c \simeq 0.023)$ for the only topological model is ~ 0.012 while for the topological and geometrical model, at $t_c \simeq 0.0065$ it is ~ 0.003 i.e. a factor four smaller in magnitude and of the same order of magnitude than the observed decrease in transition temperature. Upon melting, the appearance and proliferation of defects in the only topological defects induces high strain on the elastic network. Geometrical defects present in the topological and geometrical model, by allowing the release of this high strain in the elastic network, are the main responsible (an increase in entropy coming from the bond entropy contribution present in our model could also play a secondary role) of the dramatic decrease of the melting temperature. This observation is quite supportive of the idea that the geometrical defects are the main responsible of the thermodynamical phase transition. In our picture the topological defects could be only a side consequence of the creation of the relevant excitations (geometrical) to the melting transition. Moreover, the transition temperatures are similar, at a given pressure, to those obtained in the case when only geometrical defects are allowed, enhancing the idea that the melting is mainly driven by the geometrical excitations.

Finally, we can estimate the relative variation in volume upon melting. For the only topological model, $\Delta v/v_S$, with $\Delta v = v_L - v_S$, v_L and v_S being respectively the volume of the liquid and solid phase is of the order of 0.02. It is significantly lower than the WCA simulations where $\Delta v/v_S \simeq 0.033$. It is also possible to estimate the change of entropy on melting from the condition for chemical equilibrium, $\Delta g = 0 = \Delta u - T\Delta s + P\Delta v$, where g is the Gibbs free energy per particle, u is the internal energy per particle and s is the entropy per particle. This leads to

$$\Delta s = \frac{1}{T}(\Delta u + P\Delta v) \quad (9)$$

We found Δs which vary from $0.8k_B$ at $p = 0.1$ and decrease to $0.55k_B$ at $p = 0$. The entropy variation is larger than the one usually found in WCA simulation, in DRP or in theory. The WCA simulation give, for $T = 0.6$, $\Delta s \simeq 0.4k_B$ which is the same order of magnitude than the results obtained in other 2D simulations, in DRP and in theory.

For the topological and geometrical model, the relative variation of volume on melting is slightly more important than for the case when only topological defects are allowed. We found a value in better agreement with the WCA simulation, $\Delta v/v_S \simeq 0.033$ (at $p = 0.08$ with $N = 1024$), due to the presence of the square like polygons. Using equation 9 we compute the variation of entropy on melting and we found a value quite similar to the case with

only topological defects, i.e. $\Delta s \simeq 0.77$. As mentioned before, the melting transition and crystal-expanded crystal transition present in the only geometrical model occur at temperatures of the same order of magnitude due to the presence of the geometrical fluctuation. However, the slope of the (X_h -EX) boundary is steeper than the slope of the (X_h -L) boundary. Using the relationship $dp/dt = \Delta s/\Delta t$ combined to the fact that the change in volume upon transition is similar for both models, lead to a change of entropy on melting larger when topological defects are allowed.

LIQUID STRUCTURES

The structure of the dense liquid exhibited by the elastic model is investigated in more detail with the larger system, $N = 1024$, at a reduced pressure $p = 0.08$ for both the only topological model and the topological and geometrical model. This relatively high pressure have been chosen in order to avoid the complication in the comparison introduced by the presence of quasicrystalline and squarelike crystal structure. In order to study the microscopic structure of the dense liquid we chose a reduced temperature t_l such that $(t_l - t_c)/t_c \simeq Cst$, the constant being the same for both the only topological model and the topological and geometrical model. In addition, we compare the dense liquid structure to the WCA liquid structure obtained at a density ρ_l . Figure 8 shows the radial pair correlation function and the bond-orientational correlation function for the topological and geometrical model at a reduced temperature $t = 0.007$. The correlation functions exhibits the typical behavior of a dense liquid with short-range positional and bond-orientational order (within the finite-size effects).

Upon the solid-liquid transition, the number of topological and geometrical defects increase dramatically, as shown on Figures 5a,b for the only topological model and the topological and geometrical model. We can notice that the number of topological defects is significantly higher when bond breaking is allowed (Table I). This is mainly due to the fact that a broken bond is free to flip without energy penalty in our model. This is a feature which is present in the particle-based system for which a very slight motion of neighbor particles leads to the creation of a defect quadrupole (see Figure 1). It could also be due to stress release or screening effects which favor the proliferation of topological defects at a lower energetical cost.

For the topological and geometrical model, the number of broken bonds (and then the number of square-like geometrical defects) in the liquid phase is around 28%. By comparison, the WCA liquid exhibits only 15% of broken bonds at $\rho_l = 0.80$ (the chosen density for our comparison), this number increasing deeper in the liquid phase (22% at $\rho_l = 0.70$ [1]).

On Figures 6a and 6b, we notice that the topological defects are highly correlated forming chains of alternating signs. The geometrical defects are also highly correlated and aggregate in different structures. It is of interest to try to make a vertex classification in which vertices are classified according to the sequence of polygons (squares and triangles) present around a given vertex. Square-triangle (ST) tiling are models used to describe liquids [15, 16, 17] and more recently some dodecagonal quasicrystals [24, 25, 26, 27]. There are four vertex type, hereafter referred as type A, B, C and D which are involved in ST plane tiling [1]. Our results, displayed on Table II show that vertex of type B and C are quite common in our model. In this sense, the local arrangement of 3 and 4-sides polygons appears to be strongly conditioned by tiling rules with a clear tendency for the 3 and 4-sides polygons to form structure characteristics of ST tiling. It is worth noticing that the vertex types listed in Table II account respectively for 99.8% and 66% of the total vertex types present in the elastic model (topological and geometrical) and the WCA liquid. The relatively low percentage obtained for the WCA liquid is due to the fact that vertex types involving tiles with more than four sides are present (for example vertex types involving one hexagonal tile account for 22% of the total vertex types present). Our model exhibits a tendency to have more type B and C vertex than type A and D. If the population of vertex D is also low in the case of the WCA, the vertex A (corresponding to a perfect local solidlike region) are more numerous than in the elastic network model. This trend is increased further by decreasing the overall network rigidity.

Of course, there is also many violation of the tiling rule. The vertex types E, F, G, H, and I correspond to tiling faults and they account respectively for 25%, 43% and 27% of the total vertex type respectively for the elastic model and the WCA liquid. Vertex types E and F appear to be the most common tiling faults with type E most probable than type F for both the elastic model and the WCA liquid. From a vertex type point of view, the elastic model exhibits features which are close from those of the WCA liquid. The elastic model comes closer to the WCA liquid but the network rigidity seems still slightly too small to be able to capture one important feature of the WCA liquid, i.e the fact that the most common vertex remains the type A, since more type B and C are present in our model.

We can see the dense liquid as a generalized tiling model in which the tiles (triangles and squares) are deformable, leading to the creation of tiling faults. A measure of the rate of deformation of a perfect ST tile can be obtain by

computing the tiling charge associated to each vertex in our system. This can be done by computing [1]:

$$c_\alpha = 6 \left(\sum_{j=1}^{n_\alpha} \left(\frac{1}{2} - \frac{1}{p_j} \right) - 1 \right) \quad (10)$$

where the sum ranges over the n_α polygons which are around a vertex α , and p_j is the number of side of the j th polygon.

It is easy to verify that the ‘quantum’ of tiling charge is $1/10$ in generalized tilings consisting of tiles having six of fewer sides, and we are expressing the tiling charge in tenth. For example vertices E and F have a tiling charge of $\pm 1/2$, corresponding to ± 5 tenths. Vertices corresponding to the perfect ST tilings, i.e, types A, B, C and D have a zero tiling charge. In our model, due to the restriction we imposed on the nature of the allowed geometrical defects, only tiling charge of strengths 0, ± 5 and ± 10 are possible. We notice that in our system (Table III), the larger tiling charges account only for $\sim 0.2\%$ of the total tiling charge, suggesting that the local arrangements of polygons are strongly conditioned by tiling rules. There is a strong tendency for polygons to aggregate into structures which minimize the tiling charge around the vertices. Then, the geometrical defects have attractive, anisotropic interactions (due to their shape) that cause them to aggregate in a way that the tiling charge at a given vertex is minimized. Then the emerging picture is that the solid-liquid transition is the result of the proliferation and condensation of the geometrical defects into grain-boundary like structure.

Figures ??a,b reveal extensive regions of sixfold order in the dense WCA liquid. The typical size of these solid-like regions increases rapidly near the freezing density. The spatial aggregation of topological defects, evident on Figures 6a,b is directly related to the other prominent feature of the dense liquid shown on Figures ??a,b i.e. the existence of the large solidlike regions which appear as rafts of nearly hexagonal Voronoi cells. This dramatic spatial inhomogeneity is a consequence of the defect condensation transition which induce the melting transition and which is seen as the qualitative key feature for a microscopic understanding of a 2D dense liquid. The same behavior have been observed in the WCA liquid.

The solidlike clusters are interesting not only by themselves but also and mainly because they are a very important feature of the structure of a dense liquid and then, will play an important role on the resulting properties of the liquid, in particular on the transport properties like viscosity. Contemporary liquid state theory is incapable of predicting the detailed characteristics of such solid-like fluctuations.

Figure 9a show an example, for the only topological model in the dense liquid phase, of the cluster size distribution $n_s = N_s/N$ where N_s is the number of cluster of size s and N is the total number of particle in the system. Due to the usual normalization used in percolation theory, $\sum_s n_s = N_c/N$, N_c being the total number of ordered clusters. The solid clusters were identified by using the criterion that the local six-fold order parameter satisfy $|\psi_6| \geq 0.75$. We found that the whole distributions are quite well described by the functional form:

$$n_s = A s^{-\tau_s} \exp(-s/\xi_s) \quad (11)$$

This is the form roughly predicted by the Fisher droplet model [30] of condensation and which represents a special case of the scaling *ansatz* used in percolation theory [31, 32]. We have a power law behavior for small cluster size, and a crossover towards an exponential behavior for large cluster size. The fit to this functional form are quite good with however systematic deviation for large s . This deviation at large s is more significant in the topological and geometrical model than in the only topological model.

For the topological only model, τ_s varies in the range $1.3 - 1.5$ decreasing with decreased temperature, while in the topological and geometrical model τ_s varies in the range $1.2 - 1.3$ and exhibits a relatively smaller variation with a decrease in temperature. The only topological model bears more features with the WCA fluid, which exhibits values of τ_s in the range $1.2 - 1.5$ decreasing with decreasing density. It is interesting to notice that single percolation models exhibit a constant value of τ_s for varying site or bond occupation probabilities. Though the interpretation of τ_s is not clear, it is probably connected to the geometry of the boundaries between ordered regions and then, to the tiling rules governing the dense liquid.

In the same way, for the topological only model, ξ_s (which characterizes the typical size of the ordered clusters, lies in the range $20 - 150$, decreasing with decreasing temperature while ξ_s varies in the range $\xi_s = 5$ to $\xi_s = 10$, decreasing with decreasing temperature for the topological and geometrical model. In comparison, the WCA fluid exhibits a divergence near the freezing transition. This divergence has been attributed to a finite-size effects and is connected to the presence of large-size clusters which will be of large but finite in an infinite system but which are in the system used spanning the entire simulation box. Such effect doesn't seem to happen in our case.

In conclusion, for a finite system, n_s consists of two parts: a size-independant portion at small s and a size-dependant part at large s which develops near freezing.

More detailed informations can be obtain by computing the shape of the clusters by calculating their radius of gyration which is related to their size s by :

$$R_g = \sqrt{\frac{1}{n_s} \sum_{j=1}^{n_s} (\mathbf{r}_j - \mathbf{r}_{\text{cm}})^2} \propto s^{1/D_f} \quad (12)$$

where the sum runs over the j particles at position \mathbf{r}_j inside the given cluster and \mathbf{r}_{cm} is the center of mass of the cluster. D_f is the fractal dimension of the cluster, a value of $D_f = 2$ or close to 2 indicate a smooth rounded cluster while a significantly lower value indicates a rough cluster shape. To perform this analysis and due to the periodic boundary conditions the spanning clusters are identified and discarded. Figure 9b shows the distribution function for the radius of gyration R_g as a function of the cluster size s for the only topological model and in the dense liquid phase. A fit to the functional form gives the range of variation of D_f with the temperature. In the only topological model D_f varies in the range $D_f = 1.5$ to $D_f = 1.75$ near the freezing point, while in the topological and geometrical model, D_f varies in a range from $D_f = 1.6$ to $D_f = 1.9$ near freezing. For comparison, the WCA liquid exhibit a fractal dimension D_f varying in th range $D_f = 1.6$ to $D_f = 1.85$ near the freezing density. In the three cases, the same general qualitative feature is present: the solid clusters have a much smoother interface with the surrounding liquid near the freezing point than deeper inside the dense liquid phase. In addition, on a more quantitative point of view, it seems that the topological and geometrical model gives cluster shape in closer agreement with the WCA liquid than the topological only case. In particular the shape of the solid clusters is far smoother near freezing for the topological and geometrical model than for the only topological model.

CONCLUSION

We have study a simple elastic network model in order to be able to probe the relative role of the two fundamental excitations that, in our opinion, are important for the melting transition. Phase diagrams obtained when only geometrical defects are present exhibits 2 crystal phases with hexagonal symmetry and different density as well as a dodecagonal quasicrystalline phase. When topological defects are allowed a transition between a solid and a liquid occurs. The topological and geometrical model exhibits in addition a rich phase behavior with hexagonal crystal, dodecagonal crystal, square crystal and liquid phases. The main result is that the solid-liquid transition temperature exhibited by the model in which geometrical defects are allowed (in addition of topological defects) is decreased by a factor 3 to 4 with the transition temperature exhibited in the model where geometrical defects are forbidden. Evidently, geometrical defects stabilize the liquid phase with respect to the solid phase by releasing the high strain present in the elastic network when only topological defects are present. This observation is quite supportive of the idea that if topological defects are responsible for the loss of long range positional and bond-orientational order, geometrical defects contribute significantly to the thermodynamics of the phase transition.

This work was supported by NSF MRSEC Grant DMR 98-09555.

INTERACTION PARAMETERS

The KT temperature transition is expressed by:

$$k_B T = \frac{\overline{K}}{16\pi} \quad (13)$$

where \overline{K} is the bare-elastic constant and can be expressed as a function of the Lamé coefficients of the 2D solid [28]:

$$\overline{K} = \frac{4\mu B}{\mu + B} \quad (14)$$

where $B = -A(\partial P/\partial A)$ is the bulk modulus, and μ is the shear modulus expressed by [29]:

$$\mu = -\frac{A'}{A}(1 + \epsilon)^{-1}\mathcal{P}(1 + \epsilon^T)^{-1} \quad (15)$$

where A' is the deformed volume, ϵ is the strain tensor, ϵ^T its transposed and \mathcal{P} is the microscopic stress tensor defined as :

$$\mathcal{P}_{\alpha\beta} = \frac{1}{A'} \sum_i \sum_{j>i} r_{ij\alpha} F_{ij\beta} \quad (16)$$

with $r_{ij\alpha} = r_{i\alpha} - r_{j\alpha}$ is the α -component of the distance between particles i and j and $F_{ij\beta}$ is the β -component of the force due to the particle i on particle j .

In order to have a rough analytical idea of the magnitude of the predicted KT transition we compute the Lamé coefficients in the framework of our model at $T = 0$, i.e. considering that we have a perfect 2D-triangular solid lattice. Moreover we assume that the pure shear strain is infinitesimal.

At the first order in strain magnitude, the bulk and shear modulus are expressed in dimensionless variables by :

$$B = \frac{\sqrt{3}}{2} \left(1 + \frac{p}{\sqrt{3}} \right) \quad (17)$$

$$\mu = \frac{p}{2} + \frac{\sqrt{3}}{2} \left(1 + 3K \left(1 + \frac{p}{\sqrt{3}} \right) \right) \quad (18)$$

Then, the dimensionless KT transition temperature $t_{KT} = k_B T_{KT} / K_r a^2$ is :

$$t_{KT} = \frac{p + \sqrt{3} \left(1 + 3K \left(1 + \frac{p}{\sqrt{3}} \right)^2 \right)}{1 + \frac{3}{2} K \left(1 + \frac{p}{\sqrt{3}} \right)} \quad (19)$$

-
- [1] M. A. Glaser and N. A. Clark, *Adv. Chem. Phys.* **83**, 543 (1993).
 - [2] J. D. Bernal, *Nature* **183**, 141 (1959).
 - [3] J. D. Bernal, *Nature* **185**, 68 (1960).
 - [4] J. D. Bernal, *Proc. R. Soc. A* **280**, 299 (1964).
 - [5] J. D. Bernal, in *Liquids: Structure, Properties, Solid Interactions*, T. J. Hughel, Ed. (Elsevier, Amsterdam, 1965), p.25.
 - [6] J. P. Hansen and I. R. McDonald, *Theory of Simple Liquids*, (Academic Press, London, 1986)
 - [7] P. C. Hohenberg, *Phys. Rev.* **158**, 383 (1967)
 - [8] N. D. Mermin and H. Wagner, *Phys. Rev. Lett.* **17**, 1133 (1966)
 - [9] N. D. Mermin, *Phys. Rev.* **176**, 250 (1968)
 - [10] J. M. Kosterlitz and D. J. Thouless, *J. Phys. C* **5**, L124 (1972)
 - [11] J. M. Kosterlitz and D. J. Thouless, *J. Phys. C* **6**, 1181 (1973)
 - [12] B. I. Halperin and D. R. Nelson, *Phys. Rev. Lett.* **41**, 121 (1978)
 - [13] D. R. Nelson and B. I. Halperin, *Phys. Rev. B* **19**, 2457 (1979)
 - [14] A. P. Young, *Phys. Rev. B* **19**, 1855 (1979)
 - [15] R. Collins, *Proc. Phys. Soc.* **83**, 553 (1964)
 - [16] H. Kawamura, *Prog. Theor. Phys.* **70**, 352 (1983)
 - [17] Y. M. Yi and Z. C. Guo, *J. Phys.: Condens. Matter* **1**, 1731 (1989)
 - [18] J. M. Ziman, *Models of Disorder* (Cambridge University Press, Cambridge, England, 1979)
 - [19] J. L. Finney, *Mater. Sci. Eng.* **23**, 207 (1976)
 - [20] G. F. Voronoi and J. Reine, *Angew. Math.* **134**, 198 (1908)
 - [21] A. N. Berker and D. Anderman, *J. Appl. Phys.* **53**, 7923 (1982)
 - [22] B. Nienhuis, A. N. Berker, E. K. Riedel and M. Schick, *Phys. Rev. Lett.* **43**, 737 (1979)
 - [23] N. Metropolis, A. W. Rosenbluth, M. N. Rosenbluth, A. N. Teller, and E. Teller, *J. Chem. Phys.* **21**, 1087 (1953)
 - [24] H. Chen, D. X. Li and K. H. Kuo, *Phys. Rev. Lett.* **60**, 1645 (1988)

- [25] P. W. Leung, C. L. Henley and G. V. Chester, *Phys. Rev. B* **39**, 446 (1989)
- [26] Q. B. Yang and W. D. Wei, *Phys. Rev. Lett.* **58**, 1020 (1987)
- [27] K. H. Kuoi, Y. C. Feng and H. Chen, *Phys. Rev. Lett.* **61**, 1740 (1988)
- [28] J. Friedel, *Dislocations* (Pergamon Press, London, 1964)
- [29] D. Frenkel, in *Simple Molecular Systems at Very High Density* edited by A. Polian, P. Loubeyre, and N. Boccara (Plenum, New York, 1988)
- [30] M. E. Fisher, *Physics* **3**, 255 (1967)
- [31] D. Stauffer, *Phys. Rep.* **54**, 1 (1979)
- [32] D. Stauffer, *Introduction to Percolation Theory* (Taylor & Francis, London, 1985)

FIG. 1: Voronoi construction for two nearly square arrangements of particles, showing how a small displacement of the particles can create a disclination quadrupole (right) from a configuration with no disclination. Schematic representation of the holes created by a geometrical non topological defect (left).

FIG. 2: Schematic representation of the discrete elastic model, in which each node is connected to its nearest-neighbors with an elastic spring of equilibrium length a and elastic constant K_r . In addition, bond-angle springs with equilibrium bending angle θ_p and elastic constant K_θ are used between adjacent springs.

FIG. 3: Illustration of the MC moves performed on the springs (a) bond flipping to mimic the creation of topological defects (arrising from the unbinding of a quadrupole); (b) bond breaking to mimic the creation of a geometrical defect.

FIG. 4: Phase diagrams obtained for a system of $N = 100$ nodes with $K = 0.1$ as a function of temperature t and pressure p (a) only geometrical defects; (b) only topological defects, the upper dashed line being an estimate of the Kosterlitz-Thouless transition temperature; (c) both topological and geometrical defects. X_h represents an hexagonal crystal phase, X_s a square crystal phase, QX a dodecagonal quasicrystal phase and L the dense liquid phase.

FIG. 5: Representative evolution of various order parameters (top) and defects distribution (bottom), as a function of the reduced temperature, for the topological and geometrical model, with $N = 1024$ at $p = 0.01$. Top: $|\Psi_4|^2$ (\bullet), $|\Psi_6|^2$ (\square); $|\Psi_{12}|^2$ (\triangle); Bottom: topological defects (5 and 7-coordination nodes) (\bullet); geometrical defects (broken bonds) (\triangle). The vertical lines represent the location of X_h - QX , QX - X_s and X_s - L phase transitions.

FIG. 7: Representative configurations for the only geometrical model (top) and for the only topological model (bottom), for $N = 1024$. From top to bottom and from left to right: dodecagonal crystal (QX) at $p = 0.02$, $t = 0.0064$; expanded crystal (EX) at $p = 0.02$, $t = 0.008$; dense liquid (L) at $p = 0.08$, $t = 0.024$ ($t_c \sim 0.023$); dense liquid (L) at $p = 0.08$, $t = 0.028$. Red circle represent -1 topological defects and blue circle represent +1 topological defects. Only non-broken bonds are represented.

FIG. 8: Typical radial correlation function in the dense liquid phase of the topological and geometrical model, $N = 1024$, $p = 0.08$, $t = 0.007$. Top: radial pair correlation function $g(r)$; Bottom: radial bond-orientational order correlation function $g-6(r)$.

FIG. 9: Distribution functions, in the case of the only topological model with $K = 0.1$ and $t = 0.025$, of (a) the cluster size n_s . The solid line represents a fit to Equation (18); (b) the cluster radius of gyration. The solid line represents a fit to Equation (19).

Coordination number	topological	geometrical	only topological	WCA liquid
3		0	0	0
4		0	0	4.31×10^{-4}
5	0.2284		0.1020	0.1513
6	0.5432		0.7960	0.6987
7	0.2284		0.1020	0.1469
8	0		0	2.63×10^{-3}
9	0		0	2.8×10^{-8}

TABLE II: Probabilities of occurrence of various vertex type

Vertex type	Topological and geometrical	WCA liquid
A	0.116	0.158
B	0.288	0.123
C	0.319	0.106
D	0.021	0.005
E	0.082	0.111
F	0.073	0.102
G	0.045	0.027
H	0.027	0.017
I	0.027	0.015

FIG. 6: Representative configurations for the topological and geometrical model for $N = 1024$. From top to bottom and from left to right: hexagonal crystal (X_h) at $p = 0.08$, $t = 0.005$; square crystal (X_s) at $p = 0.01$, $t = 0.007$; dodecagonal quasicrystal (QX) at $p = 0.04$, $t = 0.0056$; dense liquid (L) at $p = 0.08$, $t = 0.007$. Red circle represent -1 topological defects and blue circle represent +1 topological defects. Only non-broken bonds are represented.

TABLE III: Probabilities of occurrence of various values of the tiling charge

Tiling charge (in tenths)	Topological and geometrical	WCA liquid
-10	9×10^{-3}	5.67×10^{-3}
-9	0	2.25×10^{-3}
-7	0	0.0378
-6	0	3.13×10^{-4}
-5	0.1269	0.1462
-4	0	9.6×10^{-3}
-2	0	0.1056
0	0.7447	0.4017
1	0	8.26×10^{-3}
3	0	0.0901
4	0	5.7×10^{-4}
5	0.1263	0.1413
6	0	8.53×10^{-3}
8	0	0.0224
9	0	1.16×10^{-4}
10	0.0012	0.0107

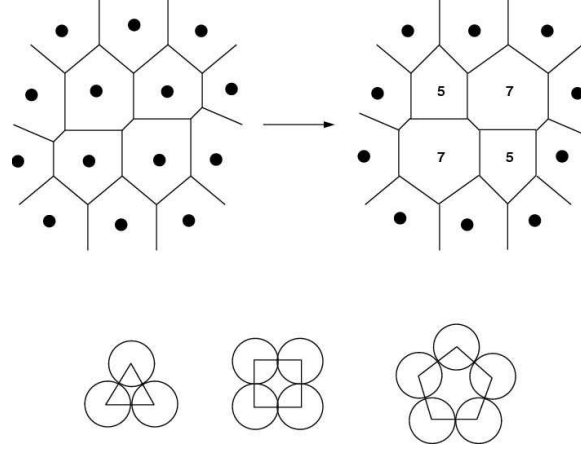


FIG. 1:

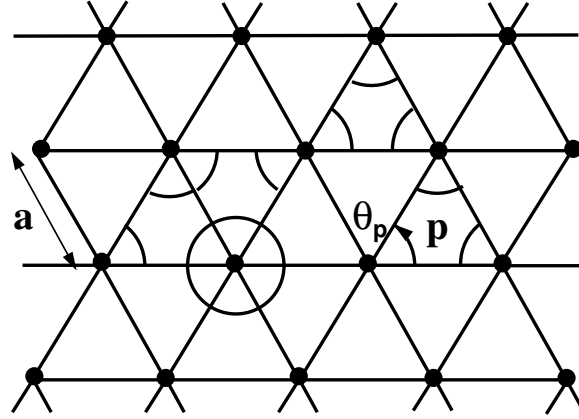


FIG. 2:

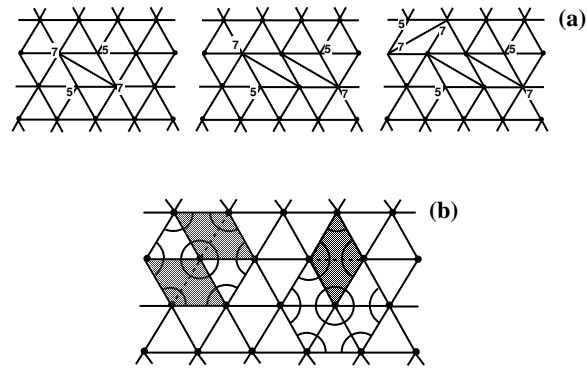


FIG. 3:

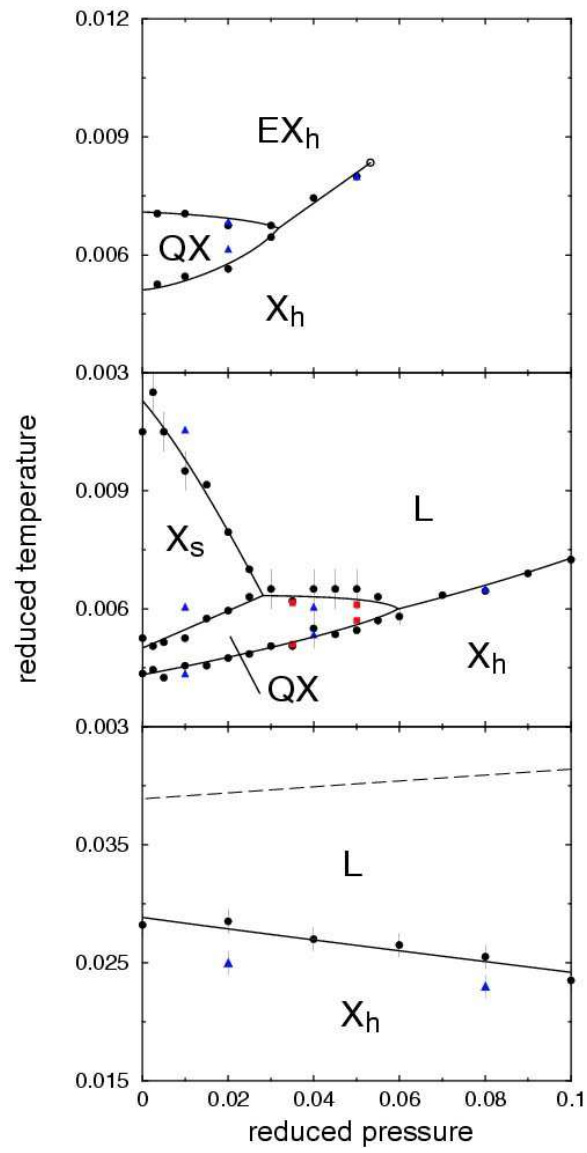


FIG. 4:

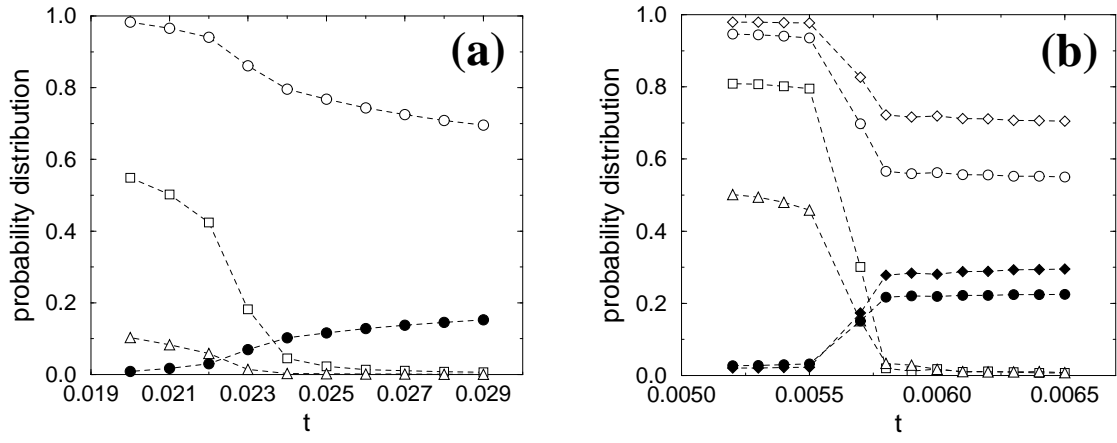


FIG. 5:

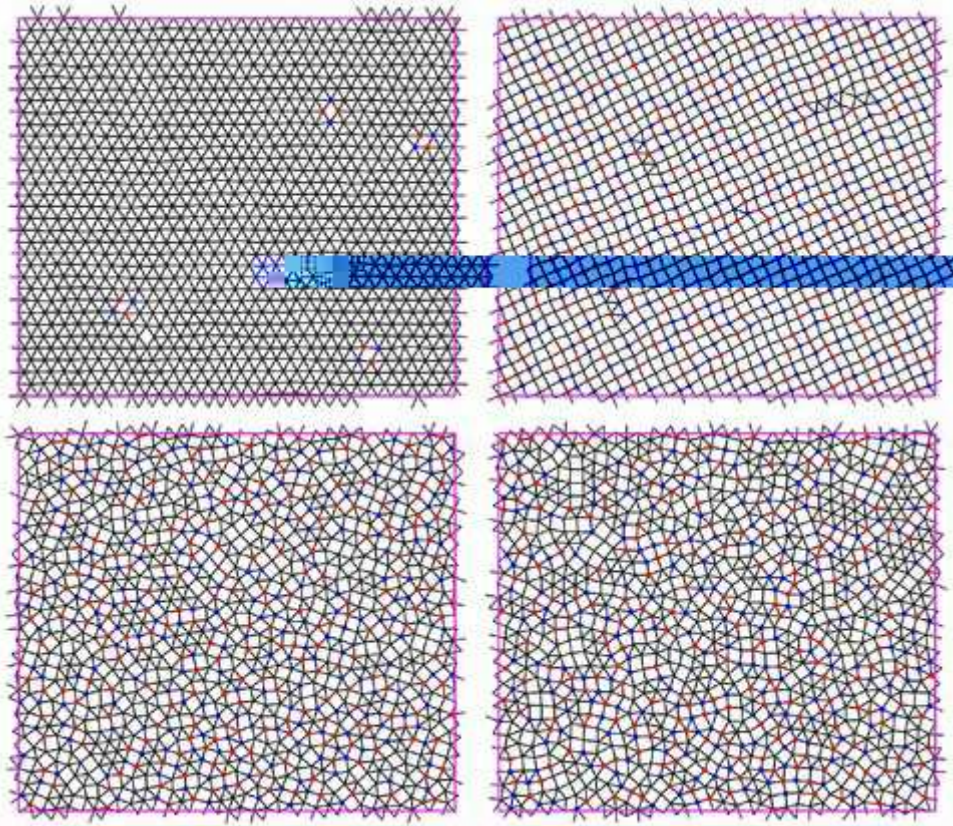


FIG. 6:

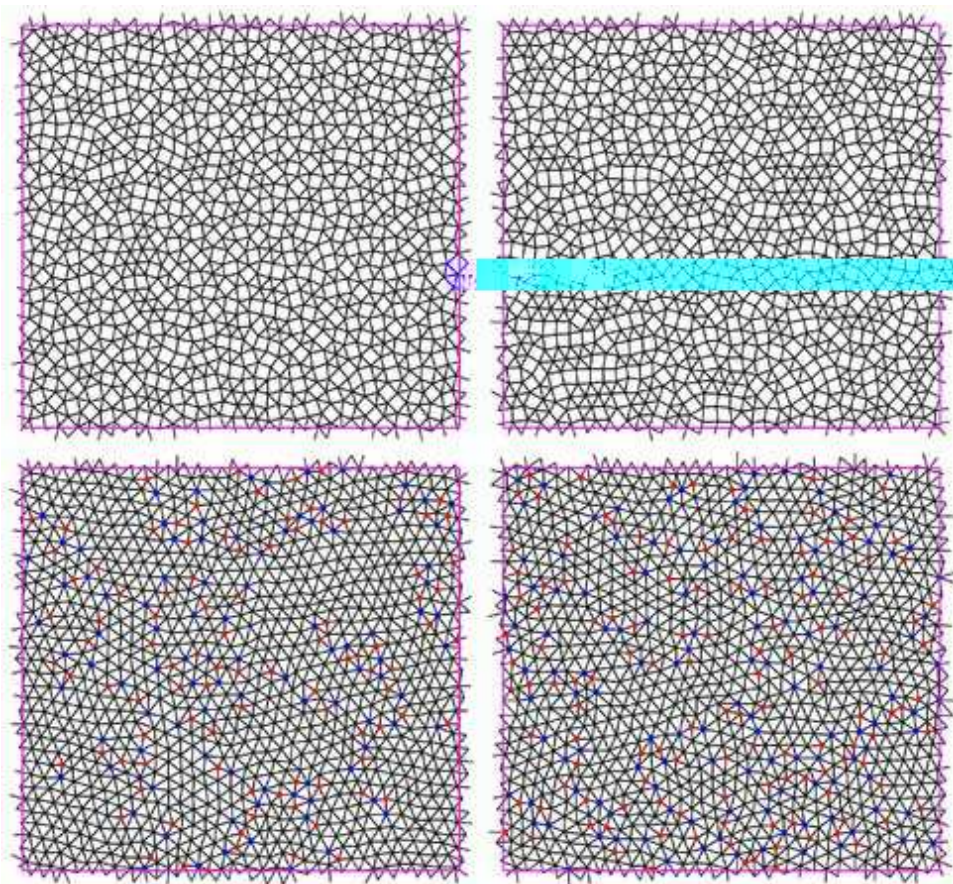


FIG. 7:

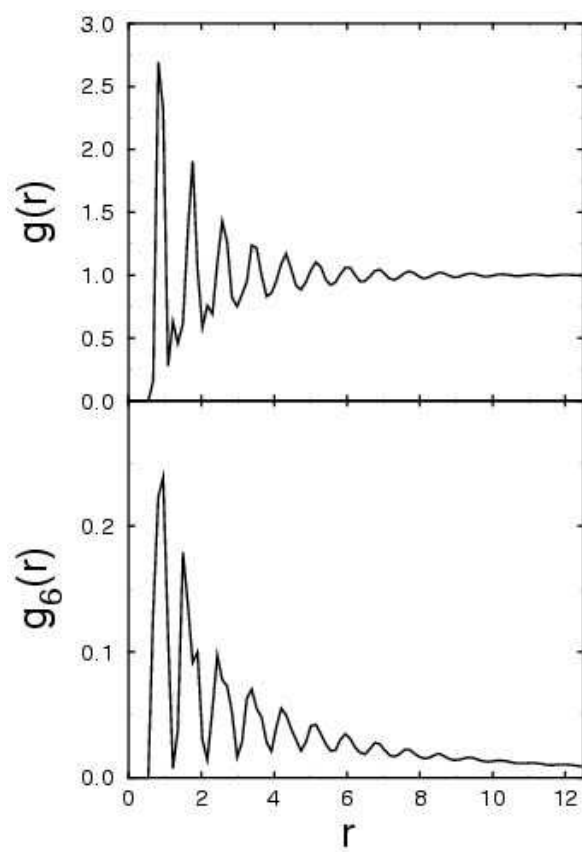


FIG. 8:

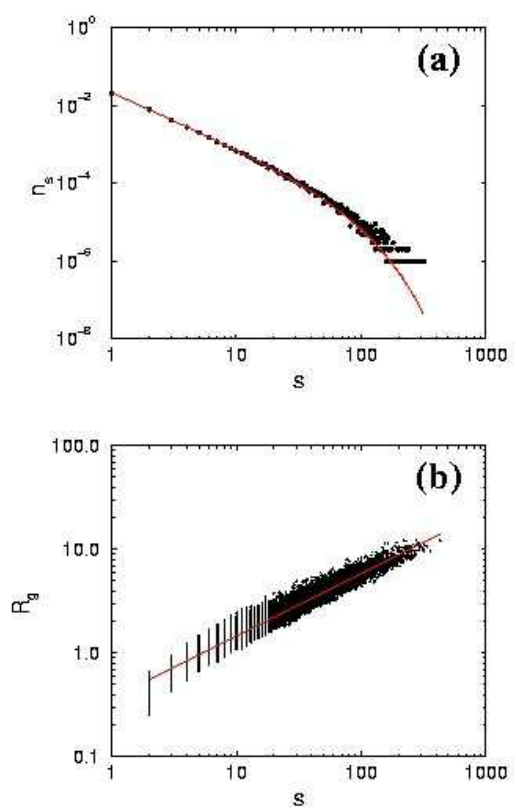


FIG. 9:

